Applied Catalysis B: Environmental 111–112 (2012) 126–132

Contents lists available at SciVerse ScienceDirect

Applied Catalysis B: Environmental

journal homepage: www.elsevier.com/locate/apcatb

Enhancing visible-light-induced photocatalytic activity by coupling with wide-band-gap semiconductor: A case study on Bi_2WO_6/TiO_2

Jiehui Xu, Wenzhong Wang*, Songmei Sun, Lu Wang

State Key Laboratory of High Performance Ceramics and Superfine Microstructure, Shanghai Institute of Ceramics, Chinese Academy of Sciences, 1295 Dingxi Road, Shanghai 200050, PR China

ARTICLE INFO

Article history:
Received 20 June 2011
Received in revised form
14 September 2011
Accepted 21 September 2011
Available online 28 September 2011

Keywords:
Bi_2WO_6/TiO_2
Photocatalysis
Visible-light
High activity

ABSTRACT

The composites of different semiconductors based on the nanoscale coupling effect for photocatalytic application has been a challenging yet very important research topic. Bi_2WO_6 and TiO_2, the two most extensively studied photocatalysts, were successfully coupled via a facile one-step hydrothermal process. The as-prepared Bi_2WO_6/TiO_2 possessed enhanced visible-light-induced activity in photocatalytic degradation of contaminants in aqueous/gaseous phases compared with those of the sole Bi_2WO_6 or TiO_2. The versatile Bi_2WO_6/TiO_2 photocatalyst also exhibited long-time recyclable ability for the contaminants degradation under visible irradiation ($\lambda > 420$ nm) of Xenon lamp or household fluorescent lamp. The photoluminescence and electrochemical impedance spectroscopy are both adopted to analyze the physical properties of the photogenerated carriers and it was found that the separation of photogenerated carriers of Bi_2WO_6 has been largely promoted after being coupled with wide-band-gap semiconductor TiO_2. This work could be extended to the design of other composite photocatalyst with the purpose of enhancing activity by coupling suitable wide and narrow band-gap semiconductors, which is inspiring for the practical environmental purification.

1. Introduction

Photocatalysis is particularly attractive for environmental applications, in line with the rules of Green Chemistry defined by Anastas (1998). Since the first report including the term "photocatalysis" [1,2], decades of efforts have been devoted to the development of photocatalysts with the aim of effectively utilizing solar energy for practical application. However, a general limitation of the photocatalytic process is the low quantum efficiencies caused by two critical factors [3], which are the competition between recombination and transfer of photogenerated charge carrier and the insufficient utilization of solar energy. Considerable efforts have been made to suppress the recombination and hence to enhance the charge carrier separation and the overall efficiency, including modification of the physicochemical properties of the semiconductor materials, such as particle size, surface area, porosity and crystallinity, and optimization of the experimental conditions during photocatalytic reactions, such as pH values, illumination conditions and catalyst loading [4–7]. To utilize solar energy more efficiently, the idea of using multiple-band-gap cells with the purpose of capturing a greater fraction of the solar spectrum has motivated much work in the field of photovoltaic solar cells [8,9], but only recently has this idea been applied in the photocatalysis. Coupling narrow-band-gap semiconductors, such as CdS, Fe_2O_3 and WO_3 being straightforward choices, with wide-band-gap semiconductors like TiO_2 does not only enhance the optical absorption abilities of the catalysts by extending the absorption range of the solar spectrum but also facilitate separation of the photogenerated carriers under the internal field induced by the different electronic band structures of matching semiconductors [10–13]. Herein, we take the case of coupling bismuth tungstate (Bi_2WO_6, band gap = 2.8 eV) with titanium dioxide (TiO_2, band gap = 3.2 eV) for an example to shed light on the idea of enhancing the activity of visible-light-driven photocatalyst (Bi_2WO_6) and extending the spectral response range of the wide-band-gap semiconductor (TiO_2).

Bi_2WO_6 with layered structure of the perovskite-like slab of WO_6 [14], which possesses excellent intrinsic physical and chemical properties, has been demonstrated to be a promising visible-light-driven photocatalyst for its activity of O_2 evolution from water and dye decomposition [14,15]. Extensive studies have been performed to tailor the micro-/nanostructures of Bi_2WO_6 to improve the photocatalytic activity as far as possible, including nanoparticles, nanoplates, and complex superstructures (solid and hollow spheres, octahedron, and mesoporous structure, etc.) [16–19]. In order to further improve the photocatalytic activity of Bi_2WO_6, some work has been reported by coupling Bi_2WO_6 with wide-band-gap semiconductors like TiO_2, the most well-known photocatalyst with high efficiency [20–22]. Attributed to

* Corresponding author. Fax: +86 21 5241 3122.
E-mail address: wzwang@mail.sic.ac.cn (W. Wang).

0926-3373/$ – see front matter © 2011 Elsevier B.V. All rights reserved.
doi:10.1016/j.apcatb.2011.09.025

the coupling effects of TiO_2, these composites of Bi_2WO_6 and TiO_2 have exhibited enhanced activities in photocatalytic degradation of organic contaminants. However, few investigations were carried on the mechanism of the enhanced photocatalytic activity and insufficient evidence was given. Recognizing the potential application of the Bi_2WO_6/TiO_2 system, we coupled Bi_2WO_6 with Degussa P25, which is reviewed to possess the best photocatalytic performances with maximum quantum yields among various oxides and chalcogenides [23]. The properties of the obtained composite photocatalyst were evaluated by photocatalytic degradation of contaminants in aqueous/gaseous phases under visible irradiation ($\lambda > 420$ nm) of Xenon lamp or household fluorescent lamp. Moreover, we aimed to approach the possible mechanism of the improved activity based on the analysis of photoluminescence (PL) and electrochemical impedance spectroscopy (EIS).

2. Experimental

2.1. Preparation of Bi_2WO_6/TiO_2 photocatalysts

All the chemicals were analytical grade reagents from Shanghai Chemical Company and used without further purification. P25 titanium dioxide (approximately 80% anatase and 20% rutile structure) was provided by the Degussa Company. The composite catalysts were synthesized by a facile one-step hydrothermal process. Since P25 is a commercial catalyst, the powders were activated in the nitric acid solution before use. In a typical hydrothermal synthesis procedure, different mass ratios of TiO_2 (15%, 25% and 35%) were well dispersed in diluted nitrite acid (HNO_3) by sonication. $Bi(NO_3)_3{\cdot}5H_2O$ and $Na_2WO_4{\cdot}2H_2O$, in a molar ratio of 2:1, were added in the TiO_2 suspension in turn. After sufficient reaction, pH value of the mixed solution was adjusted to 5 by sodium hydroxide solution. Then the suspension was added into a 50 mL Teflon-lined autoclave with a stainless steel tank and heated at 160 °C for 18 h. Afterwards, the samples obtained were rinsed with de-ionized water and anhydrous ethanol and then oven-dried at 60 °C for 4 h.

2.2. Characterization of Bi_2WO_6/TiO_2 photocatalysts

The purity and crystallinity of the as-prepared Bi_2WO_6/TiO_2 powders were characterized by powder X-ray diffraction (XRD) with a Rigaku D/MAX 2250 V diffractometer using monochromatized Cu Kα ($\lambda = 0.15418$ nm) radiation under 40 kV and 100 mA and scanning over the range of $20^\circ \le 2\theta \le 80^\circ$. The morphologies and microstructures characterizations were performed on the scanning electron microscopy (SEM, JEOL JSM-6700F) and transmission electron microscopy (TEM, JEOL JEM-2100F, accelerating voltage 200 kV). High-resolution transmission electron microscopy analysis used the Digital Micrograph software (Gatan Inc.). UV–vis diffuse reflectance spectra (DRS) of the samples were obtained on an UV–vis spectrophotometer (Hitachi U-3010) using $BaSO_4$ as the reference. The photoluminescence spectra of the samples were recorded with a PerkinElmer LS55.

Photocatalytic activities of the samples were evaluated by the degradation of simulated contaminants under the irradiation of a 500 W Xe lamp with a 420 nm cutoff filter and a fluorescent lamp (24 W, Philips Lighting Company). For the decolorization of RhB, 0.1 g of photocatalyst was added into 100 mL of RhB solution (10^{-5} mol/L) and stirred in the dark for 4 h before illumination to ensure the establishment of an adsorption–desorption equilibrium between the photocatalyst and RhB. At 1 min intervals, the absorption of a 3 mL of sample solution was recorded on a Hitachi U-3010 UV–vis spectrophotometer. For the degradation of aqueous ammonia, 0.1 g of photocatalyst was added into 100 mL of NH_4Cl solution, of which the pH value is adjusted to 10.8 by aqueous NaOH. Before illumination, the solution was stirred in the dark for 4 h in order to reach the adsorption–desorption equilibrium between the photocatalyst and $[NH_4^+/NH_3]$. The concentration of $[NH_4^+/NH_3]$ was estimated before and after the treatment using the Nesster's reagent colorimetric method. For the degradation of acetaldehyde (CH_3CHO), 0.3 g of photocatalyst was placed at the bottom of a gas-closed reactor with a quartz window at room temperature (capacity 600 mL). The reaction gas mixture (1 atm) consisted of 100 ppm CH_3CHO and N_2 balance gas. Prior to irradiation, the reaction system was equilibrated for about 60 min until no change in the concentration of CO_2 was monitored. Gaseous samples (1 mL) were periodically extracted and analyzed by a gas chromatograph (GC) equipped with a flame ionization detector (N_2 carrier) and a catalytic conversion furnace.

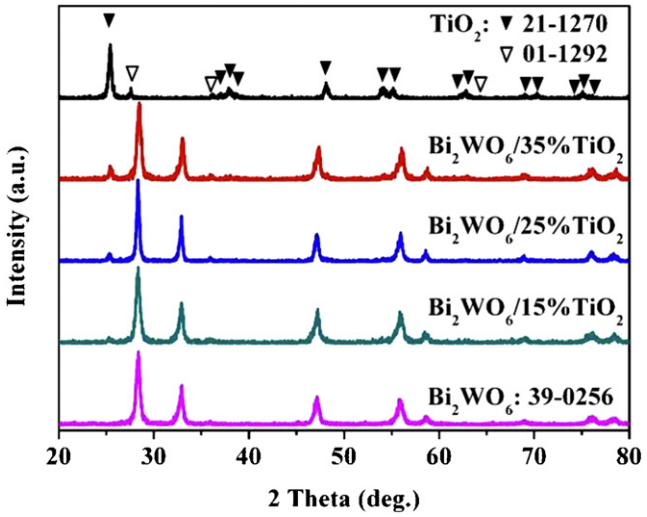

Fig. 1. XRD patterns of the Bi_2WO_6/TiO_2 with different ratios of TiO_2.

The electrochemical studies were performed on a CHI 660D electrochemical system (Shanghai, China) using a standard three-electrode cell with a working electrode, a platinum wire counter electrode, and a saturated calomel electrode (SCE) reference electrode. The working electrodes were prepared by dip-coating: Briefly, 10 mg of photocatalyst was suspended in 10 mL of ethanol to produce the slurry, which was then dip-coated on a 15 mm × 25 mm fluorine-doped tin oxide (FTO) glass electrode. Electrodes were subsequently dried at 353 K for 2 days. Photoelectrochemical properties were measured with a 500 W Xe lamp with a 420 nm cutoff filter. The electrochemical impedance spectroscopy was carried out at the open circuit potential. A sinusoidal ac perturbation of 5 mV was applied to the electrode over the frequency range 0.1–10^4 Hz. During all of the measurements, the electrolyte was 0.5 mol/L Na_2SO_4 solution.

3. Result and discussion

3.1. Preparation and characterizations of Bi_2WO_6/TiO_2 photocatalysts

The phase and composition of the Bi_2WO_6/TiO_2 photocatalysts with different mass ratios of TiO_2 to Bi_2WO_6 were given in Fig. 1. In comparison, the XRD patterns of sole Bi_2WO_6 and TiO_2 samples were offered. All the diffraction peaks can be indexed to orthorhombic phased Bi_2WO_6 (JCPDS card No.39-0256) and mixed anatase (JCPDS card No.21-1270) and rutile phased (JCPDS card No.01-1292) TiO_2. The diffraction profiles reveal that both Bi_2WO_6 and TiO_2 powder are well-crystallized and the broad diffraction peaks imply that the crystalline grains are on nanoscale. With

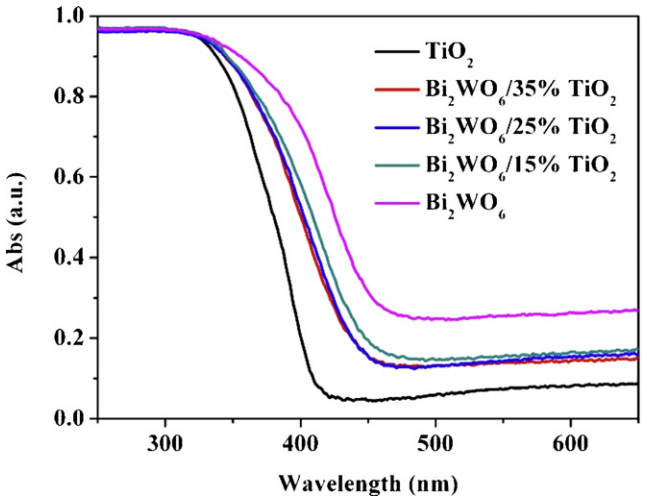

Fig. 2. UV–vis diffuse reflectance spectra of the Bi_2WO_6/TiO_2 with different ratios of TiO_2.

an increasing amount of TiO_2, the relative intensity of anatase and rutile TiO_2 phase increased accordingly. The diffuse-reflection spectra of the Bi_2WO_6/TiO_2 photocatalysts with different mass ratios of TiO_2 are depicted in Fig. 2. With the increasing ratio of Bi_2WO_6, the absorption edge of Bi_2WO_6/TiO_2 red shifted to longer wavelength within the range of visible-light, with the spectral response range of TiO_2 being extended. Bi_2WO_6 sample showed an absorption edge around 480 nm, which could be responsible for the visible-light induced photocatalytic activity.

The morphology of the composite photocatalyst was studied by the microscope images. A representative TEM image (Fig. 3a) when the mass ratio of TiO_2 was 25% demonstrated that the typical structure of the Bi_2WO_6/TiO_2 nanocomposite consisted of TiO_2 nanoparticles and Bi_2WO_6 nanosheets. Although the particles were slightly agglomerated, owing to the lack of any stabilizing surfactants, the nanoparticles of TiO_2 adhering to the Bi_2WO_6 nanosheets could be clearly distinguishable (Fig. 3b). The selected-area electron diffraction (SAED) pattern for the [0 1 0] zone axis recorded at one rectangle nanosheet exhibits a regular and clear diffraction spot array (Fig. 3d), revealing the single-crystal nature of the nanosheet. The other dispersed spots marked as 1, 2, 3, etc. were the diffraction spots from Bragg reflections of TiO_2, which are not regular or clear enough to determine.

To further investigate the influence of TiO_2 on the morphological evolution process of the Bi_2WO_6 and the nanocomposite, the bare Bi_2WO_6 without composition of TiO_2 was also synthesized by the same hydrothermal method. For comparison of the different formation processes, time-dependent experiments were carried out by extracting products at different reaction stages. Fig. 4 shows a series of SEM image of the precursor and products by varying the

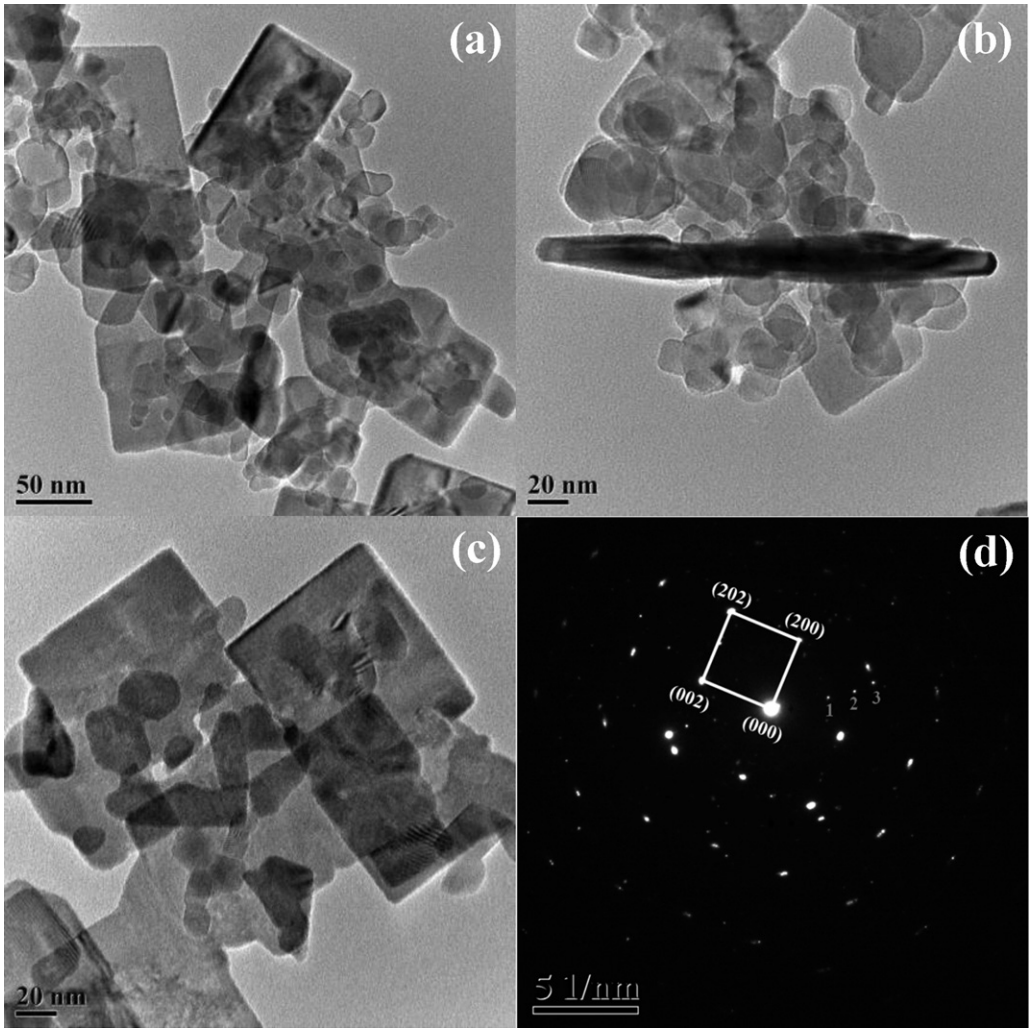

Fig. 3. TEM images (a–c) and SAED image (d) of the Bi_2WO_6/TiO_2 sample with 25% TiO_2.

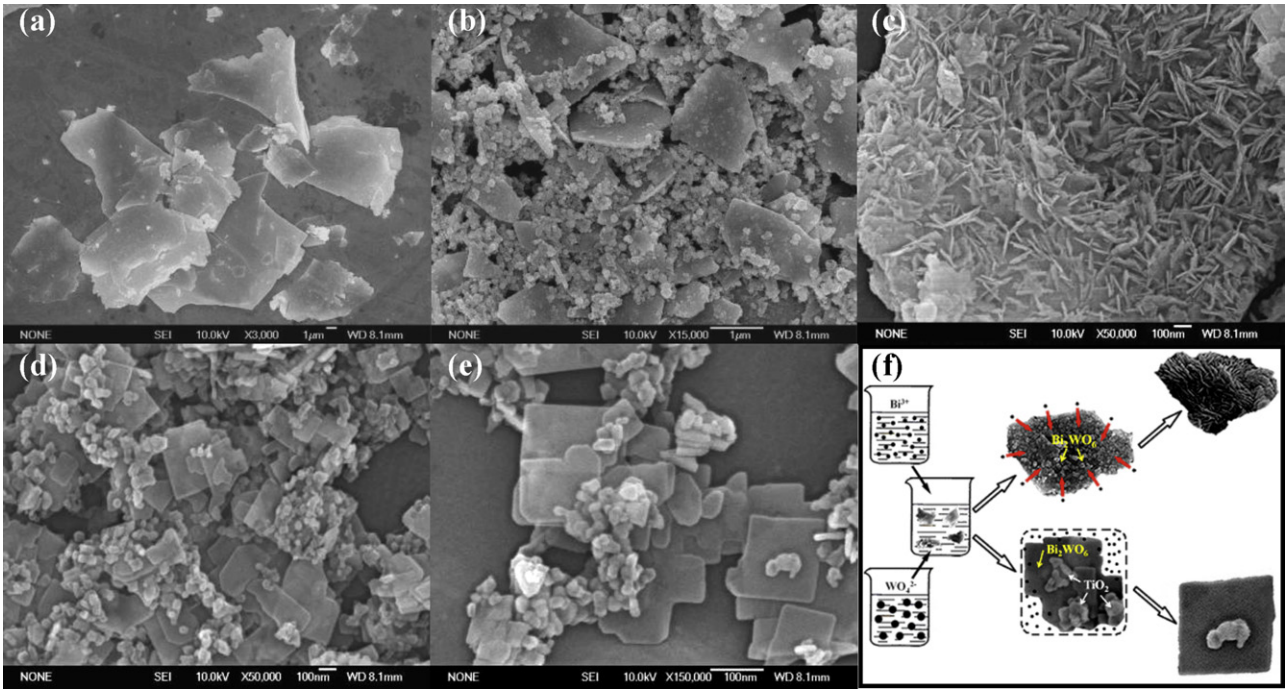

Fig. 4. SEM images of Bi_2WO_6 and Bi_2WO_6/TiO_2 samples for different hydrothermal time. (a) Bi_2WO_6 and Bi_2WO_6/TiO_2 0 h, (b) Bi_2WO_6 3 h, (c) Bi_2WO_6 18 h, (d) Bi_2WO_6/TiO_2 3 h, (e) Bi_2WO_6/TiO_2 18 h. (f) Different synthesis pathways between Bi_2WO_6 and Bi_2WO_6/TiO_2 samples.

reaction time from 0 h to 3 h and 18 h in the synthesis processes of both bare Bi_2WO_6 and Bi_2WO_6/TiO_2 composite. At the initial stage, the flake-like precursor of Bi_2WO_6 by mixing $Bi(NO_3)_3{\cdot}5H_2O$ and $Na_2WO_4{\cdot}2H_2O$ was formed in amorphous state (Fig. 4a). Afterwards, the small quantity of residual reactants in the bulk solution underwent different growing routes. For the bare Bi_2WO_6, the residual reactants of Bi and W formed amorphous nanoparticles and occupied on the active sites of the Bi_2WO_6 flake precursors (Fig. 4b). With the time going, they aggregated into ultra thin flakes to minimize the surface area. In the advanced stages of the growth, the larger plates were assembled by the crossed thin flakes on the surface (Fig. 4c). However, in the formation of the Bi_2WO_6/TiO_2 composite, TiO_2 occupied on the active sites instead of the Bi_2WO_6 amorphous nanoparticles (Fig. 4d). At the same time, the residual reactants of Bi and W in the bulk solution were intended for the growth of nearly perfect Bi_2WO_6 single crystal (Fig. 4e). The different synthesis pathways between bare Bi_2WO_6 and Bi_2WO_6/TiO_2 samples were illustrated in Fig. 4f.

3.2. Photocatalytic performance of Bi_2WO_6/TiO_2 photocatalysts

The photocatalytic activities of the Bi_2WO_6/TiO_2 composite with different ratios of TiO_2 were evaluated by the degradation of rhodamine B (RhB) dye in water (10^{-5} mol/L) under visible-light irradiation ($\lambda > 420$ nm). It was compared to that of the sole Bi_2WO_6 and TiO_2 photocatalysts. Fig. 5a shows the photocatalytic degradation curve of RhB as a function of time. The first-order linear relationship was revealed by the plots of C/C_0 vs irradiation time, where C is the concentration of RhB at the irradiation time t and the C_0 is the initial concentration. The sample with 25% TiO_2 demonstrated the highest photocatalytic activity in degradation of RhB, nearly 100% RhB was degraded in 5 min under illumination. The photocatalytic performance did not increase linearly with the ratio of TiO_2 in the nanocomposite. At lower ratio, the introduction of TiO_2 enhanced the photocatalytic activity by promoting the separation of photogenerated holes and electrons. With the increasing amount of TiO_2, the active adsorption and degradation sites on both Bi_2WO_6 nanosheets and TiO_2 nanoparticles were reduced due to the chemical connection between them, resulting in the decrease of activity of the nanocomposite. In addition, to distinguish the direct photolysis and the adsorption of RhB dyes on the nanocomposite, contrast experiments proceeded under the same conditions. The blank test confirmed that RhB was hardly degraded under visible-light in the absence of catalysts and only slightly absorbed in dark, indicating that the photolysis and adsorption action of catalysts can be ignored. The stability of the photocatalytic performance of the Bi_2WO_6/TiO_2 catalyst, which is an important factor in practical application, was evaluated. The circulating runs of the photocatalytic degradation of RhB by the $Bi_2WO_6/25\%TiO_2$ sample under visible-light were checked (Fig. 5b). The photocatalytic activity did not exhibit any obvious loss after five recycles for the photodegradation of RhB, revealing the excellent stability of Bi_2WO_6/TiO_2 catalyst and the TiO_2 nanoparticles were firmly connected to the Bi_2WO_6 nanosheets.

To further confirm the versatile properties of the as-prepared Bi_2WO_6/TiO_2 photocatalysts and eliminate the photosensitive effect of RhB, aqueous ammonium/ammonia [NH_4^+/NH_3] and gaseous acetaldehyde (CH_3CHO) were selected to evaluate the photocatalytic activity under household fluorescent light. The fluorescent lamp, which is common in household illumination, offers a new promising source for the application of photocatalysis in indoor environments purification because of its safety, long lifetime, and efficient electricity to light conversion. The aqueous [NH_4^+/NH_3] is a major nitrogen-containing pollutant, with the production of NO_2^-/NO_3^- or N_2 by degradation. An initial concentration of 10 mg/L [NH_4^+/NH_3] at pH 10.8 was used throughout this study [24,25]. As shown in Fig. 6a, the concentration of [NH_4^+/NH_3] decreases from the initial 10 mg/L to approximately 0.31 mg/L in the presence of the Bi_2WO_6/TiO_2 photocatalysts under irradiation for 3 h. More than 95% of [NH_4^+/NH_3] were degraded. The [NH_4^+/NH_3] degradation rates by sole Bi_2WO_6 and TiO_2 were also investigated. Only 66% and 25% of [NH_4^+/NH_3] were degraded after irradiated for 3 h in the presence of sole Bi_2WO_6 and TiO_2

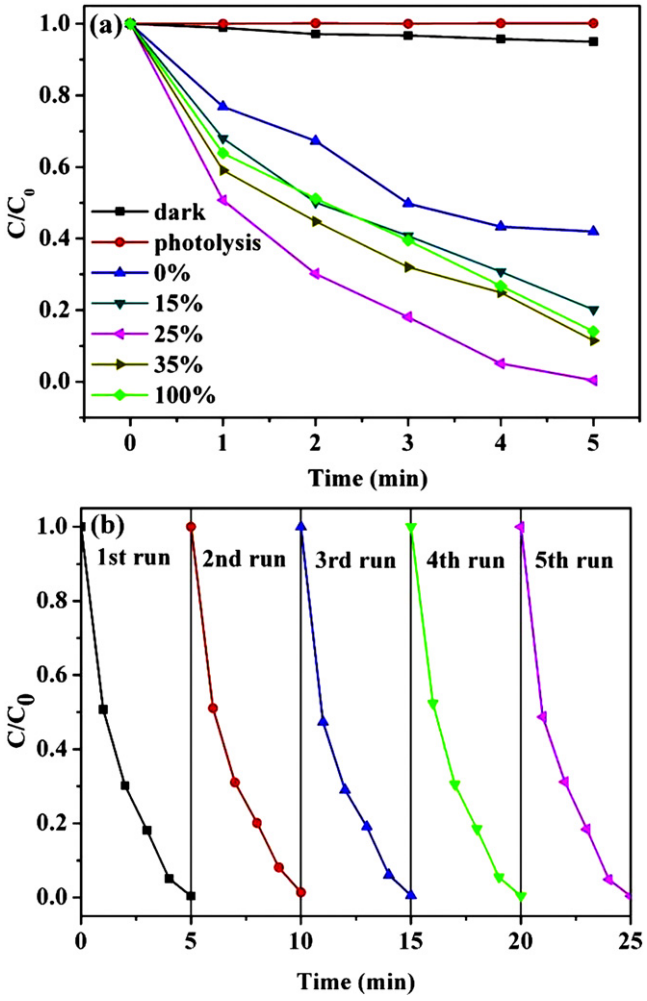

Fig. 5. (a) RhB degradation in the presence of the Bi_2WO_6/TiO_2 samples with different ratios of TiO_2 under visible-light. (b) Cycling experiment of the photocatalytic degradation of RhB in the presence of Bi_2WO_6/TiO_2 sample with 25% TiO_2 under visible-light.

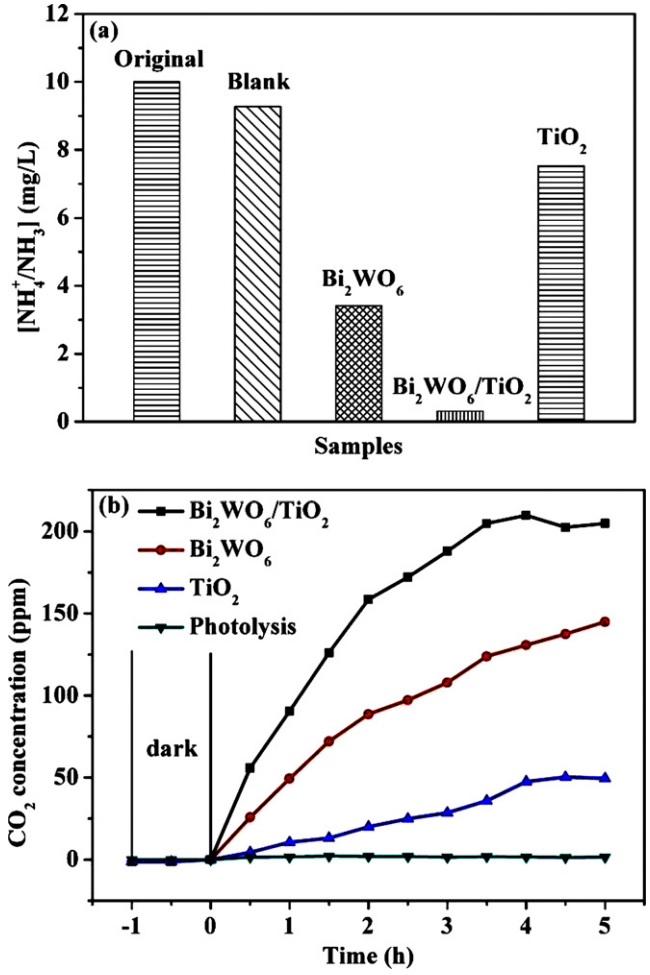

Fig. 6. $[NH_4^+/NH_3]$ (a) and acetaldehyde (b) degradation in the presence of Bi_2WO_6, TiO_2 and Bi_2WO_6/TiO_2 under the irradiation of fluorescent lamp.

respectively. In addition, a blank experiment was implemented without the photocatalyst in order to make sure the removal of aqueous $[NH_4^+/NH_3]$ by Bi_2WO_6/TiO_2 sample was not ascribed to a photolysis process or the volatilization of NH_3. The result revealed that the concentration of $[NH_4^+/NH_3]$ was only decreased by less than 10% after irradiation, indicating the real photocatalytic ability on $[NH_4^+/NH_3]$ degradation by the as-prepared samples.

Besides the $[NH_4^+/NH_3]$ decomposition, the photocatalytic degradation of acetaldehyde, a typical indoor air contamination with no light absorption during photodegradation process, was also performed under the irradiation of fluorescent light. Since it is also a common intermediate during photocatalytic oxidation of other organic compounds ranging from alkanes to alcohols, the mineralization of acetaldehyde is significant to the application of photocatalysis in deep purification. It was revealed that acetaldehyde was degraded by the samples with an obvious production of CO_2 (Fig. 6b). The rate of CO_2 evolution over Bi_2WO_6/TiO_2 composite photocatalyst was much higher than that of sole Bi_2WO_6 and TiO_2. Since the proportion of UV light in the fluorescent lamp is quite low, the degradation rate of acetaldehyde was much lower than that of Bi_2WO_6 samples. The blank test performed simultaneously showed that no self-decomposition existed, which strongly confirmed the effect of photocatalytic degradation by the Bi_2WO_6/TiO_2 photocatalyst. The above experiments have shown the excellent performance and stability of the as-prepared Bi_2WO_6/TiO_2 photocatalysts in the degradation of organic and inorganic contaminants in aqueous/gaseous phases.

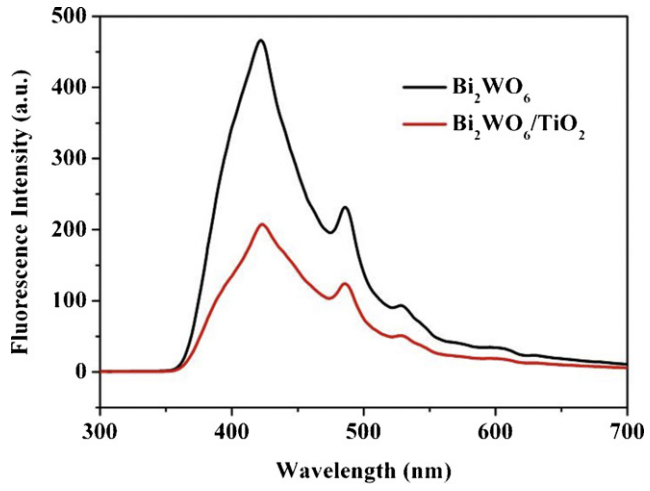

Fig. 7. Photoluminescence spectra measured at room temperature for Bi_2WO_6 and Bi_2WO_6/TiO_2. The excitation wavelength was 390 nm.

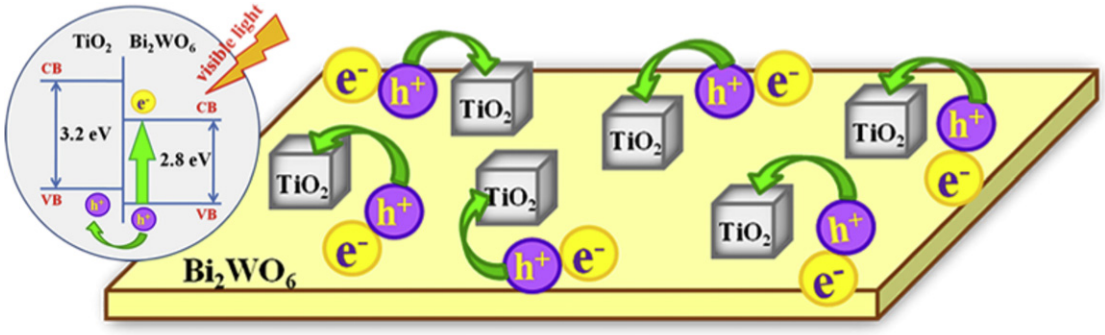

Scheme 1. Schematic diagram for energy band matching and migration and separation of electron–hole pairs in the coupled Bi_2WO_6/TiO_2 photocatalyst.

3.3. Approaching to the mechanism

As discussed above, the Bi_2WO_6/TiO_2 composite photocatalyst exhibited enhanced photocatalytic activity under both visible irradiation and household illumination. The reason should be closely attributed to the interaction between Bi_2WO_6 and TiO_2, which increased the mobility of photogenerated carriers in the photocatalyst. To confirm the effect of the interaction on the photogenerated electrons and holes, photoluminescence and electrochemical impedance spectroscopy were investigated. Since photoluminescence emission arises from the recombination of free carriers, the PL spectra is subservient to investigate the migration, transfer and recombination processes of the photogenerated electron–hole pairs in a semiconductor [26,27]. Fig. 7 shows the PL spectra of sole Bi_2WO_6 and Bi_2WO_6/TiO_2 composite in the range of 300–700 nm excited by the light with wavelength of 390 nm. Bi_2WO_6 has a broad blue–green emission peak at 420–530 nm [28]. Three intense emission peaks appeared at 423, 485, and 528 nm, respectively in the spectra of sole Bi_2WO_6. The position of the emission peaks of Bi_2WO_6 after being coupled with TiO_2 on the surface remained almost unchanged, suggesting that the interaction between TiO_2 and Bi_2WO_6 was chemical absorption. A significant decrease in the intensity of PL spectra of Bi_2WO_6/TiO_2 was observed compared to that of sole Bi_2WO_6. The weaker intensity of the peak represents the lower recombination probability of free charges. It indicates that coupling with TiO_2 could effectively inhibit the recombination of photogenerated electron–hole pairs of Bi_2WO_6, which is helpful for the separation of photogenerated charge carriers.

Furthermore, electrochemical impedance spectroscopy was also used to investigate the photogenerated charge separations process on the as-prepared samples. Fig. 8 shows EIS response of Bi_2WO_6/FTO film and Bi_2WO_6/TiO_2/FTO film under visible-light irradiation. The radius of the arc on the EIS Nynquist plot reflects the reaction rate occurring at the surface of electrode. The arc radius on EIS Nynquist plot of Bi_2WO_6/TiO_2/FTO film was smaller than that of Bi_2WO_6/FTO film sample, which meant that an effective separation of photogenerated electron–hole pairs and fast interfacial charge transfer to the electron donor/electron acceptor occurred as suggested [29,30].

Both PL spectra and EIS have confirmed the increased migration and separation of photogenerated electrons and holes. By the introduction of wide-band-gap semiconductor TiO_2, the internal field was generated, and it promoted the electrons and holes migrating to different field directions. According to estimated E_g values of the Bi_2WO_6 and TiO_2 sample, the calculated conduction band (CB) and valence band (VB) edge potentials are displayed in Scheme 1 [31]. The VB level Bi_2WO_6 is lower by 0.353 V than that of TiO_2. In the process of photocatalysis, the electrons in the VB Bi_2WO_6 are excited to its CB under irradiation, and the holes in the VB of the Bi_2WO_6 can be transferred to that of TiO_2. The large flat sheet of Bi_2WO_6

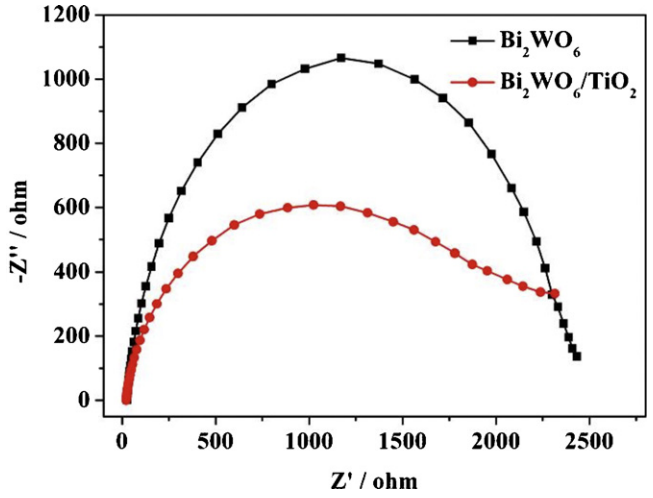

Fig. 8. EIS Nyquist plots of Bi_2WO_6 and Bi_2WO_6/TiO_2 electrodes under visible-light irradiation.

facilitates the migration of electrons and the holes incline to accumulate on the surface of TiO_2 nanoparticles. The high specific surface area of P25 (BET = 50 ± 15 m^2/g) is beneficial to the acceptance of large quantities of holes. Therefore, the photogenerated electrons and holes pairs were separated efficiently and the probability of recombination was reduced accordingly. The electrons on the surface of Bi_2WO_6 sheets and holes on the TiO_2 particles, respectively, can participate in photocatalytic reactions to directly or indirectly mineralize organic pollution, and thus the photocatalytic reaction can be enhanced greatly.

4. Conclusion

The efficient composite photocatalyst Bi_2WO_6/TiO_2 prepared by a simple one-step hydrothermal process has been presented. The coupled photocatalyst exhibited enhanced visible-light-induced activity in photocatalytic degradation of contaminants in aqueous/gaseous phases compared with those of the sole Bi_2WO_6 or TiO_2. Besides the excellent photocatalytic activity, Bi_2WO_6/TiO_2 also possesses good stability in photocatalytic performance. The possible mechanism of the increased activity in Bi_2WO_6/TiO_2 system was approached for the first time. Both PL spectra and EIS analysis revealed the introduction of TiO_2 promoted the mobility and separation of photogenerated carriers effectively and consequently enhanced the number of active electrons and holes in the photocatalytic processes. The obtained Bi_2WO_6/TiO_2 photocatalyst with excellent activity and stability presents the potential for practical application. The idea of enhancing the activity of

visible-light-driven photocatalyst by coupling with wide-band-gap semiconductor is inspiring for the research of coupled photocatalysts and their practical application in environmental purification.

Acknowledgements

This work is financially supported by the National Natural Science Foundation of China (50972155, 50902144 and 50732004), National Basic Research Program of China (2010CB933503) and Science Foundation for Youth Scholar of State Key Laboratory of High Performance Ceramics and Superfine Microstructures (SKL 200904).

References

[1] W. Doerffler, K. Hauffe, J. Catal. 3 (1964) 156–170.
[2] W. Doerffler, K. Hauffe, J. Catal. 3 (1964) 171–178.
[3] M.R. Hoffmann, S.T. Martin, W.Y. Choi, D.W. Bahnemann, Chem. Rev. 95 (1995) 69–96.
[4] X. Xu, R.J. Lu, X.F. Zhao, S.L. Xu, X.D. Lei, F.Z. Zhang, D.G. Evans, Appl. Catal. B: Environ. 102 (2011) 147–156.
[5] X. Zhao, Y.F. Zhu, Environ. Sci. Technol. 40 (2006) 3367–3372.
[6] Z.Y. Liu, X.T. Zhang, S. Nishimoto, T. Murakami, A. Fujishima, Environ. Sci. Technol. 42 (2008) 8547–8551.
[7] K. Sayama, H. Hayashi, T. Arai, M. Yanagida, T. Gunji, H. Sugihara, Appl. Catal. B: Environ. 94 (2010) 150–157.
[8] S. Licht, J. Phys. Chem. B 105 (2001) 6281–6294.
[9] S. Licht, B. Wang, T. Soga, M. Umeno, Appl. Phys. Lett. 74 (1999) 4055–4057.
[10] Y.B. Liu, H.B. Zhou, B.X. Zhou, J.H. Li, H.C. Chen, J.J. Wang, J. Bai, W.F. Shangguan, W.M. Cai, Int. J. Hydrogen Energy 36 (2011) 167–174.
[11] L.L. Peng, T.F. Xie, Y.C. Lu, H.M. Fan, D.J. Wang, Phys. Chem. Chem. Phys. 12 (2010) 8033–8041.
[12] Y.T. Kwon, K.Y. Song, W.I. Lee, G.J. Choi, Y.R. Do, J. Catal. 191 (2000) 192–199.
[13] M. Miyauchi, A.K. Nakajima, T. Watanabe, K. Hashimoto, Chem. Mater. 14 (2002) 4714–4720.
[14] J.W. Tang, Z.G. Zou, J.H. Ye, Catal. Lett. 92 (2004) 53–56.
[15] A. Kudo, S. Hijii, Chem. Lett. (1999) 1103–1104.
[16] F. Amano, K. Nogami, B. Ohtani, J. Phys. Chem. C 113 (2009) 1536–1542.
[17] H.D. Xie, D.Z. Shen, X.Q. Wang, G.Q. Shen, Mater. Chem. Phys. 103 (2007) 334–339.
[18] D.X. Wu, H.T. Zhu, C.Y. Zhang, L. Chen, Chem. Commun. 46 (2010) 7250–7252.
[19] C.Y. Wang, H. Zhang, F. Li, L.Y. Zhu, Environ. Sci. Technol. 44 (2010) 6843–6848.
[20] G. Colon, S.M. Lopez, M.C. Hidalgo, J.A. Navio, Chem. Commun. 46 (2010) 4809–4811.
[21] M. Shang, W.Z. Wang, L. Zhang, S.M. Sun, L. Wang, L. Zhou, J. Phys. Chem. C 113 (2009) 14727–14731.
[22] Y. Zhou, K. Vuille, A. Heel, G.R. Patzke, Z. Anorg. Allg. Chem. 635 (2009) 1848–1855.
[23] J.M. Herrmann, Sci. China: Chem. 53 (2010) 1831–1843.
[24] X.D. Zhu, S.R. Castleberry, M.A. Nanny, E.C. Butler, Environ. Sci. Technol. 39 (2005) 3784–3791.
[25] H.H. Ou, C.H. Liao, Y.H. Liou, J.H. Hong, S.L. Lo, Environ. Sci. Technol. 42 (2008) 4507–4512.
[26] F.B. Li, X.Z. Li, Appl. Catal. A: Gen. 228 (2002) 15–27.
[27] F.B. Li, X.Z. Li, Chemosphere 48 (2002) 1103–1111.
[28] Q. Xiao, J. Zhang, C. Xiao, X.K. Tan, Catal. Commun. 9 (2008) 1247–1253.
[29] W.H. Leng, Z. Zhang, J.Q. Zhang, C.N. Cao, J. Phys. Chem. B 109 (2005) 15008–15023.
[30] H. Liu, S.A. Cheng, M. Wu, H.J. Wu, J.Q. Zhang, W.H. Li, C.N. Cao, J. Phys. Chem. A 104 (2000) 7016–7020.
[31] M.A. Butler, J. Appl. Phys. 48 (1977) 1914–1920.